

Nonlinear modes and symmetry breaking in rotating double-well potentials

Yongyao Li^{1,2}, Wei Pang³, and Boris A. Malomed^{1*}

¹*Department of Physical Electronics, School of Electrical Engineering,
Faculty of Engineering, Tel Aviv University, Tel Aviv 69978, Israel*

²*Department of Applied Physics, South China Agricultural University, Guangzhou 510642, China*

³*Department of Experiment Teaching, Guangdong University of Technology, Guangzhou 510006, China.*

We study modes trapped in a rotating ring carrying the self-focusing (SF) or defocusing (SDF) cubic nonlinearity and double-well potential $\cos^2 \theta$, where θ is the angular coordinate. The model, based on the nonlinear Schrödinger (NLS) equation in the rotating reference frame, describes the light propagation in a twisted pipe waveguide, as well as in other optical settings, and also a Bose-Einstein condensate (BEC) trapped in a torus and dragged by the rotating potential. In the SF and SDF regimes, five and four trapped modes of different symmetries are found, respectively. The shapes and stability of the modes, and transitions between them are studied in the first rotational Brillouin zone. In the SF regime, two symmetry-breaking transitions are found, of subcritical and supercritical types. In the SDF regime, an antisymmetry-breaking transition occurs. Ground-states are identified in both the SF and SDF systems.

PACS numbers: 42.65.Tg; 03.75.Lm; 47.20.Ky; 05.45.Yv

I. INTRODUCTION

The concept of the spontaneous symmetry breaking (SSB) in nonlinear systems was introduced in Ref. [1]. Its significance has been later recognized in various physical settings, including numerous ones originating in nonlinear optics [2]-[5], Bose-Einstein condensates (BECs) [6]-[12], and degenerate fermionic gases [13]. A general analysis of the SSB phenomenology was developed too [14], which is closely related to the theory of bifurcations in nonlinear systems [15].

Fundamental manifestations of the SSB occur in nonlinear systems based on symmetric double-well potentials (DWPs) or dual-core configurations. A paradigmatic example of the latter in nonlinear optics is the twin-core nonlinear fiber, which may serve as a basis for the power-controlled optical switching [2]. DWP settings in optics were analyzed theoretically and implemented experimentally in photorefractive crystals [5]. In the realm of matter waves, main effects predicted in DWPs are Josephson oscillations [7], the asymmetric self-trapping of localized modes [8], and similar effects in binary mixtures [9, 10]. Both the Josephson and self-trapping regimes were implemented in the atomic condensate with contact repulsive interactions [11]. The SSB was also analyzed in one- and two-dimensional (1D and 2D) models of BEC trapped in dual-core configurations [12].

Another dynamical setting which has produced a number of interesting effects in media with the intrinsic nonlinearity, especially in BEC, is provided by rotating potentials. It is well known that stirring the self-repulsive condensate typically leads to the formation of vortex lattices [17], although it was found experimentally [18] and demonstrated theoretically [19] that giant vortices, rather than lattices, may also be formed under special conditions (when the centrifugal force nearly compensates the trapping harmonic-oscillator potential). On the other hand, the rotation of self-attractive condensates gives rise to several varieties of stable localized modes, such as vortices, “crescents” (mixed-vorticity states), and the so-called center-of-mass modes (quasi-solitons) [20]. Further development of this topic was achieved by the consideration of rotating lattice potentials, which can be implemented experimentally as an optical lattice induced in BEC by a broad laser beam transmitted through a revolving sieve [21], or using *twisted* photonic-crystal fibers in optics [22]. In these systems, quantum BEC states and vortex lattices have been studied [23], as well as solitons and solitary vortices depinning from the lattice when its rotation velocity exceeds a critical value [24].

A specific implementation of the latter settings is provided by the quasi-1D lattice, or a single quasi-1D potential well, revolving about its center in the 2D geometry [25]. In particular, the rotation makes it possible to create fundamental and vortical soliton in the self-repulsive medium, where, obviously, nonrotating quasi-1D potentials cannot maintain bright solitons [26]. Furthermore, the rotation of a DWP gives rise to azimuthal Bloch bands [27, 28].

*Electronic address: malomed@post.tau.ac.il

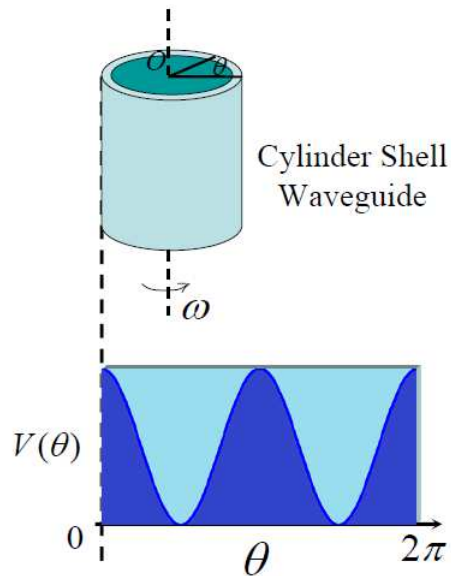


FIG. 1: (Color online) The pipe waveguide with the intrinsic potential, twisted at rate ω .

As mentioned above, the static DWP and its limit form reducing to dual-core systems are fundamental settings for the onset of the SSB [2]-[12]. A natural problem, which is the subject of the present work, is the SSB and related phenomenology, i.e., the existence and stability of symmetric, antisymmetric, and asymmetric modes, in *rotating* DWPs (recently, a revolving DWP configuration was considered in a different context in Ref. [30], as a stirrer generating vortex lattices). To analyze basic features of the phenomenology, we here concentrate on the one-dimensional DWP placed onto a rotating ring. As shown in Fig. 1, in optics this setting may be realized as a hollow pipe waveguide twisted with pitch $2\pi/\omega$, while the azimuthal modulation of the refractive index, that gives rise to the effective potential $V(\theta)$, is written into the material of the pipe. Alternatively, a *helical* potential structure can be created in a straight sheath waveguide by means of optical-induction techniques, using pump waves with the ordinary polarization in a photorefractive material (while the probe wave is to be launched in the extraordinary polarization [31]), or the method of the electromagnetically-induced transparency (EIT) [33], including its version recently proposed for supporting spatial solitons [34]. In the latter case, one can make the pipe out of Y_2SiO_5 crystal doped by Pr^{3+} (Pr:YSO) ions [35]. In either case of the use of the photorefractive material or EIT, the helical structure may be induced by a superposition of a pair of co-propagating *vortical* pump waves, with equal amplitudes, a small mismatch of the propagation constants $k_{1,2}$ ($\Delta k \equiv k_1 - k_2 \ll k_1$), and opposite vorticities ($\pm S$), which will give rise to an effective potential profile,

$$V(\theta, z) \sim r^S \cos(\Delta k \cdot z + 2S\theta), \quad (1)$$

where z is the propagation distance, while r and θ are the polar coordinates in the transverse plane. In terms of the BEC, a similar setting may be based on ring-shaped (toroidal) traps, which have been created in experiments [36] and investigated in various contexts theoretically [37]. In that case, the rotating periodic potential can be added to the toroidal trap [21], which is equivalent to the consideration of the rotating ring [28, 38].

In this work, we study basic types of trapped modes and their SSB phenomenology in the 1D rotating ring, in both cases of the self-focusing and self-defocusing (SF and SDF) cubic nonlinearities. In Sec. II we formulate the model and present analytical results, which predict a boundary between the symmetric and asymmetric modes, the analysis being possible for the small-amplitude potential and the rotation rate close to $\omega = 1/2$. Numerical results are reported in a systematic form, and are compared to the analytical predictions, in Secs. III and IV for the SF and SDF nonlinearities, respectively. The paper is concluded by Sec. IV.

II. THE MODEL AND ANALYTICAL CONSIDERATIONS

As said above, we consider the limit of a thin helical shell, which implies a fixed value of the radius in Eq. (1), $r = r_0$, that we normalize to be $r_0 = 1$. Taking the harmonic periodic potential in the form of Eq. (1) with $S = 1$,

$V(\theta, z) = 2A \cos^2(\theta - \omega z)$, the corresponding scaled nonlinear Schrödinger equation is

$$i \frac{\partial}{\partial z} \psi = \left[-\frac{1}{2} \frac{\partial^2}{\partial \theta^2} + V(\theta, z) - \sigma |\psi|^2 \right] \psi, \quad (2)$$

where $\sigma = +1$ and -1 refer to SF and SDF nonlinearities, respectively. Then, we rewrite Eq. (2) in the helical coordinate system, with $\theta' \equiv \theta - \omega z$:

$$i \frac{\partial}{\partial z} \psi = \left[-\frac{1}{2} \frac{\partial^2}{\partial \theta'^2} + i\omega \frac{\partial}{\partial \theta'} + 2A \cos^2(\theta') - \sigma |\psi|^2 \right] \psi, \quad (3)$$

where the solution domain is defined at $-\pi \leq \theta' \leq +\pi$. For the narrow toroidal BEC trap with the rotating potential, the respective Gross-Pitaevskii equation, written in the co-rotating reference frame (cf. Refs. [27, 28]), differs by replacing the propagation distance, z , with time t [29].

Stationary modes with real propagation constant $-\mu$ (in terms of the BEC, μ is the chemical potential) are sought for as $\psi(\theta', z) = \exp(-i\mu z) \phi(\theta')$, with complex function $\phi(\theta')$ obeying equation

$$\mu \phi = \left[-\frac{1}{2} \frac{d^2}{d\theta'^2} + i\omega \frac{d}{d\theta'} + 2A \cos^2(\theta') - \sigma |\phi|^2 \right] \phi. \quad (4)$$

Equation (3) conserves the total power (norm) of the field and its Hamiltonian (energy),

$$P = \int_{-\pi}^{+\pi} |\psi(\theta')|^2 d\theta', \quad (5)$$

$$H = \int_{-\pi}^{+\pi} \left[\frac{1}{2} \left| \frac{\partial \psi}{\partial \theta'} \right|^2 + \frac{i}{2} \omega \left(\psi^* \frac{\partial \psi}{\partial \theta'} - \psi \frac{\partial \psi^*}{\partial \theta'} \right) + V(\theta') |\psi|^2 - \frac{\sigma}{2} |\psi|^4 \right] d\theta', \quad (6)$$

with the asterisk stands for the complex conjugate.

The periodic boundary conditions, $V(\theta' + 2\pi) = V(\theta')$ and $\psi(\theta' + 2\pi) = \psi(\theta')$, make Eq. (3) invariant with respect to the *boost transformation*, which allows one to change the rotation speed from ω to $\omega - N$ with arbitrary integer N :

$$\psi(\theta', z; \omega - N) = \psi(\theta', z; \omega) \exp \left[-iN\theta' + i \left(\frac{1}{2} N^2 - N\omega \right) z \right], \quad (7)$$

hence the speed may be restricted to interval $0 \leq \omega < 1$. Furthermore, Eq. (3) admits an additional invariance, relating solutions for opposite signs of the rotation speed: $\psi(\theta', z; \omega) = \psi^*(\theta', -z; -\omega)$. If combined with shift $\omega \rightarrow \omega + 1$, the latter transformation implies that the solutions for the rotation speeds ω and $1 - \omega$ (with $0 < \omega < 1$) are mutually tantamount, therefore the rotation speed may be eventually restricted to interval

$$0 \leq \omega \leq 1/2, \quad (8)$$

which plays the role similar to that of the first Brillouin zone in solid-state media [39].

An analytical approach for small-amplitude modes can be developed if the amplitude of the potential in Eq. (3) is small too, $|A| \ll 1$, and ω is close to the right edge of zone (8), $\delta \equiv 1/2 - \omega \ll 1/2$. In the simplest approximation, the corresponding stationary solutions are looked for as a combination of the zeroth and first angular harmonics,

$$\phi(\theta') = a_0 + a_1 \exp(i\theta'), \quad (9)$$

where a_0 is fixed to be real, while amplitude a_1 may be complex. Indeed, setting $\omega = 1/2$, $A = 0$, and dropping the cubic term, it is obvious that Eq. (9) is an exact solution to Eq. (4). Then, under the aforementioned conditions, the substitution of ansatz (9) into Eq. (4) yields, in the first approximation (taking care of the balance of the zeroth and first harmonics in the equation), the following algebraic equations:

$$\begin{aligned} \mu a_0 &= A a_0 - \sigma a_0^3 - 2\sigma |a_1|^2 a_0, \\ \mu a_1 &= \delta a_1 - \sigma |a_1|^2 a_1 - 2\sigma a_0^2 a_1 + A a_1. \end{aligned} \quad (10)$$

First, setting $a_1 = 0$ or $a_0 = 0$ in ansatz (9) corresponds, respectively, to the CW (continuous-wave) mode, and the uniform vortical one, with $|\psi(\theta')| = \text{const}$:

$$a_1 = 0, \quad a_0^2 = \sigma(A - \mu), \quad (11)$$

$$a_0 = 0, \quad |a_1|^2 = \sigma(A - \mu + \delta) \quad (12)$$

TABLE I: Different species of stationary modes in the case of the SF nonlinearity ($\sigma = +1$), labeled by input waveforms which generate them.

Inputs	Types of modes
$\cos \theta'$	Fundamental-harmonic symmetric (FHS)
$1 + \sin \theta'$	Fundamental-harmonic asymmetric (FHA)
$\sin^2 \theta'$	Second-harmonic symmetric (2HS)
$1 + \sin \theta'$	Second-harmonic asymmetric (2HA)
$\sin \theta'$	Anti-symmetric (AnS)
$b + \sin \theta', 0 < b \leq 1$	Broken-antisymmetry (BAnS)

(recall that $\sigma^2 = 1$). In terms of full equation (3) with $A \neq 0$, these two solutions extend into non-uniform ones [with $|\psi(\theta')| \neq \text{const}$], which remain (and are categorized as) *symmetric* with respect to point $\theta' = 0$. The respective vortical mode, obtained as the extension of solution (12), is investigated in a numerical form in the next section, under the name of FHS (fundamental-harmonic symmetric) mode.

Solutions to Eqs. (10) with $a_0 a_1 \neq 0$ give rise to the species of *asymmetric* modes (categorized as FHA, i.e., fundamental-harmonic asymmetric mode, in the next section), with

$$a_0^2 = \frac{\sigma}{3}(A - \mu + 2\delta), \quad |a_1|^2 = \frac{\sigma}{3}(A - \mu - \delta). \quad (13)$$

According to Eqs. (5) and (9), the propagation constant is related to total power (5) of soliton (13), $P = 2\pi(a_0^2 + |a_1|^2)$, as follows:

$$\mu = A + \frac{\delta}{2} - \frac{3\sigma}{4\pi}P. \quad (14)$$

In particular, in the case of the SF nonlinearity, with $\sigma = +1$, Eq. (14) demonstrates that the asymmetric mode meets the Vakhitov-Kolokolov (VK) criterion, $d\mu/dP < 0$, which is a necessary stability condition for modes supported by the SF terms [40]. On the other hand, in the case of the SDF sign of the nonlinearity, $\sigma = -1$, the asymmetric mode satisfies the “anti-VK” criterion, $d\mu/dP > 0$, which, as argued in Ref. [41], may also play the role of a necessary stability condition, in the respective setting.

Further, Eq. (13) predicts a transition between the symmetric (FHS) and asymmetric (FHA) vortical modes at $a_0^2 = 0$, i.e., at $\mu = A + 2\delta$. Then, Eq. (14) yields the location of this boundary in terms of the total power, $P_{\min} = 2\pi\sigma\delta$. In view of the above-mentioned equivalence between the modes pertaining to rotation speeds $\omega = 1/2 \pm \delta$, the latter result predicts the coexistence of the FHS and FHA modes at

$$P \geq P_{\min} = 2\pi|\delta|. \quad (15)$$

Comparison of this prediction with numerical findings is presented below.

III. NUMERICAL RESULTS FOR THE SELF-FOCUSING NONLINEARITY ($\sigma = +1$)

A. Symmetric, asymmetric, and antisymmetric modes

Solutions to stationary equation (4) were constructed by means of numerical code “PCSOM” elaborated in Ref. [42]. In the SF case, the use of different input waveforms makes it possible to identify five distinct species of stationary modes, as listed in Table I.

The symmetry, asymmetry and antisymmetry of the modes designated in Table 1 is realized with respect to point $\theta' = 0$, while the solution is considered, as defined above, in the region of $-\pi \leq \theta' \leq +\pi$. Further, the fundamental or second harmonic (“FH” or “2H”, respectively) in the nomenclature adopted in the table refers to a dominant term in the Fourier decomposition of the stationary solution (which is made obvious by their shapes, see below). In particular, the stationary patterns of the FHA and 2HA types are generated by the same input in Table 1, $1 + \sin \theta'$, but in non-overlapping regions of the parameter space, (ω, A, P) , as shown below. Note also that all the inputs displayed in the table are real functions, but the numerical modes found for $\omega \neq 0$ have a complex structure.

The stability of the stationary solutions has been identified through the numerical computation of eigenvalues for infinitesimal perturbation modes. To this end, the perturbed solution was taken in the usual form,

$$\psi = e^{-i\mu z} [\phi(\theta') + u(\theta')e^{i\lambda z} + v^*(\theta')e^{-i\lambda^* z}], \quad (16)$$

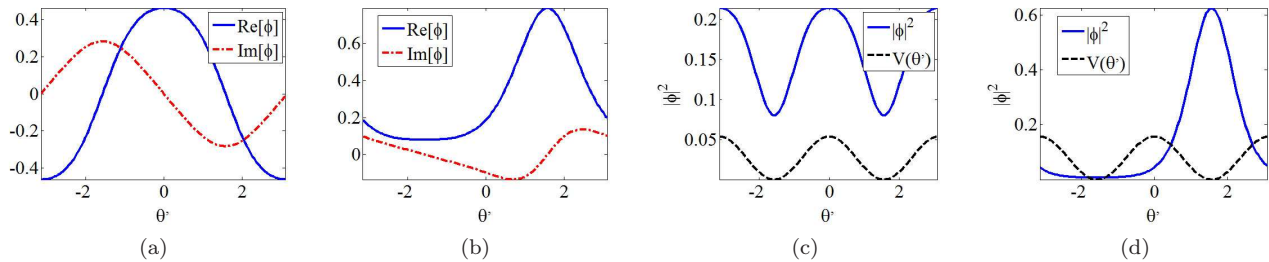


FIG. 2: (Color online) Examples of stable FHS and FHA (fundamental-harmonic symmetric and asymmetric) modes, in the case of the SF nonlinearity, corresponding to the same parameter set, $(\omega, A, P) = (0.35, 0.5, 1)$. (a,b) Real and imaginary parts of the FHS and FHA stationary solutions, respectively. (c,d) Intensity profiles of the same solutions. The dashed curves in (c) and (d), and in similar panels displayed below, depict the potential, $V(\theta') = 2A \cos^2(\theta')$.

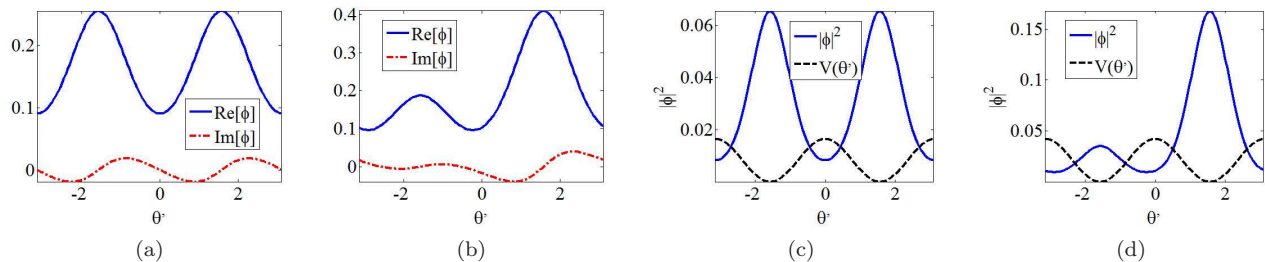


FIG. 3: (Color online) Examples of stable modes of the 2HS and 2HA (second-harmonic symmetric and asymmetric) types, in the case of the SF nonlinearity, found at sets of the parameter values $(\omega, A, P) = (0.25, 1, 0.2)$ and $(0.25, 1, 0.3)$, respectively. (a,b) Real and imaginary parts of the 2HS and 2HA stationary solutions, respectively. (c,d) Intensity profiles of the same solutions. Unlike the fundamental-harmonic modes shown in Fig. 2, these ones, based on the second harmonic, feature no bistability (coexistence of the stable modes).

where $u(\theta')$ and $v(\theta')$ are perturbation eigenmodes, and λ is the corresponding eigenfrequency. The substitution of expression (16) into Eq. (3) and linearization leads to the eigenvalue problem in the following form:

$$\begin{pmatrix} \mu - \hat{h} - i\omega \frac{\partial}{\partial \theta'} & \sigma \phi^2 \\ -\sigma (\phi^*)^2 & -\mu + \hat{h} - i\omega \frac{\partial}{\partial \theta'} \end{pmatrix} \begin{pmatrix} u \\ v \end{pmatrix} = \lambda \begin{pmatrix} u \\ v \end{pmatrix}, \quad (17)$$

where $\hat{h} = -(1/2)\partial^2/\partial\theta'^2 + 2A \cos^2(\theta') - 2\sigma|\phi|^2$ is the respective single-particle Hamiltonian. The underlying solution ϕ is stable if all the eigenvalues are real.

In the case of the SF nonlinearity, the numerical solutions reveal the existence of all the species of the modes indicated in Table 1, except for BAnS, which exist under the SDF nonlinearity, see below. Typical examples of the five species of the stationary modes which are supported by the SDF cubic term are displayed in Fig. 2-4. The analysis demonstrates that all these examples are stable. Moreover, the symmetric and asymmetric modes dominated by the fundamental harmonic, FHS and FHA, demonstrate mutual *bistability* in Fig. 2, as these stable modes coexist at common values of the parameters.

A distinctive feature of the FHS mode, which is evident in Fig. 2, is that maxima and minima of its intensity coincide with local maxima and the minima of the harmonic potential, while its FHA counterpart features an intensity maximum in one potential well, and a minimum in the other. This structure of the FHS suggests that it may correspond to a maximum, rather than minimum, of the energy (see below), but, nevertheless, this mode has a region of stability against small perturbations.

On the other hand, Figs. 3 and 4 demonstrates that both the 2HS and AnS modes have two symmetric intensity peaks trapped in the two potential wells (while local minima of the intensity coincide, quite naturally, with potential humps), hence these mode have a chance to realize a minimum of the energy (in the best case, it may be the system's ground state). The 2HA mode features a similar property in Fig. 3, but with unequal density peaks trapped in the two potential minima.

In the limit of the uniform ring (without the potential, $A = 0$) the FHS and AnS modes go over into the above-mentioned uniform vortical state (12), the 2HS pattern degenerates into the CW state (11), while the FHA mode

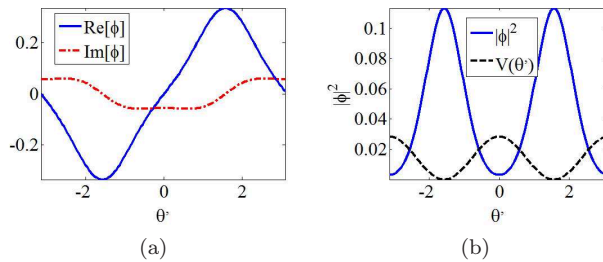


FIG. 4: (Color online) An example of a stable mode of the AnS (antisymmetric) type, at $(\omega, A, P) = (0.25, 1, 0.3)$: (a) real and imaginary parts of the stationary solution; (b) its intensity profile.

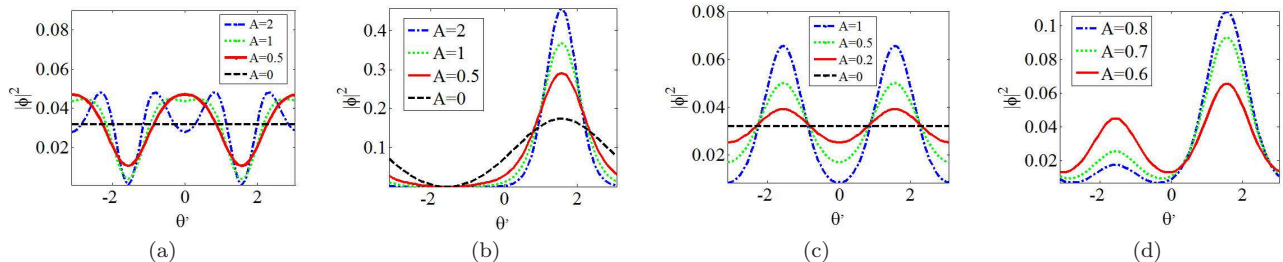


FIG. 5: (Color online) (a) The FHS mode, in the case of the SF nonlinearity with $(\omega, P) = (0.25, 0.2)$, at different values of the potential's strength, A . (b) The same for the FHA mode with $(\omega, P) = (0.5, 0.5)$. (c) The same for the 2HS mode with $(\omega, P) = (0.25, 0.2)$. (d) The same for the 2HA mode with $(\omega, P) = (0.4, 0.2)$. All the modes shown in this figure are stable.

takes the form of a 2π -periodic cnoidal-wave solution of the nonlinear Schrödinger equation (the 2HA pattern does not exist at all in the limit of $A = 0$). The evolution of the shape of the modes with the increase of A is shown in Fig. 5 [The evolution figure of AnS mode, which is not shown here, is similar to the 2HS type displayed in Fig. 5(c)].

B. Existence and stability diagrams for the different modes

Results of the systematic numerical analysis are summarized in Fig. 6, in the form of diagrams for the existence of the stable FHS and FHA modes in the plane of (P, ω) at several fixed values of amplitude A of the harmonic potential. In the blank areas, only *unstable* modes of the FHS type are found [in direct simulations they feature an oscillatory instability, which is accounted for by a quartet of complex eigenvalues generated by Eq. (17)], while the FHA modes are completely stable in their existence region.

The dashed lines in panels (a) and (b) of Fig. 6 demonstrate that Eq. (15) correctly predicts the bistability boundary at small values of $\delta \equiv 1/2 - \omega$ and P , provided that A is small enough too [recall it is the condition under which Eq. (15) was derived]. Further, the fact that vertical cuts of the panels in Fig. 6, that can be drawn through $\omega = \text{const}$, go, with the increase of the total power (P), from the region of the monostability of the FHS mode through the FHS/FHA bistability area into the monostability region of the FHA mode (at least, for ω sufficiently close to $1/2$), clearly suggests that the symmetry-breaking bifurcation of the *subcritical type*, which features the bistability [15], [2], occurs along this route. This conclusion is confirmed by a direct consideration of the numerical data (not shown here in detail).

As concerns the AnS solitons, in the case of the SF nonlinearity they do not undergo any bifurcation, and are stable in the entire region of their existence, which is shown in the (ω, P) plane for fixed values of the lattice's strength, A , in Fig. 7 [as mentioned above, at $A = 0$ the AnS mode coincides with the FHS one, hence the respective existence area is the same as the red (bottom) one in Fig. 6(a)]. From here we conclude that the stability region of the AnS mode quickly expands with the increase of A , and the FHS/FHA bistability areas in panels (b) and (c) of Fig. 6 actually support the *tristability*, as the AnS mode is stable there too.

The multistability between the three species of the modes based on the fundamental harmonic—symmetric, asymmetric, and antisymmetric ones—makes it necessary to compare their energies, which are defined as per Eq. (6). The

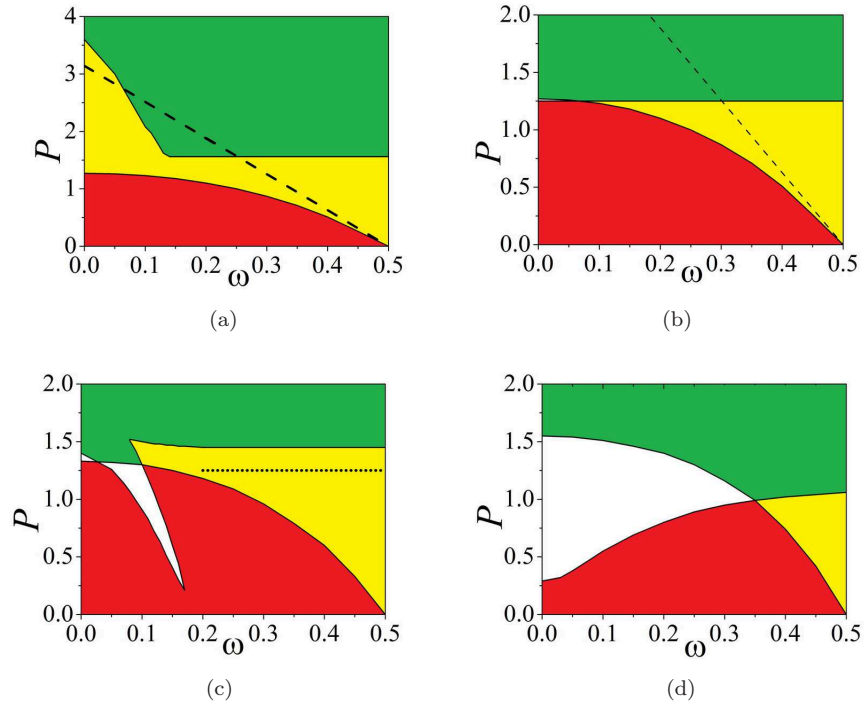


FIG. 6: (Color online) Stability diagrams for the symmetric and asymmetric modes dominated by the fundamental harmonic in the case of the SF nonlinearity, in the plane of the rotation speed (ω) and total power (P), at several fixed values of the potential's strength: (a) $A = 0$, (b) $A = 0.2$, (c) $A = 0.5$, and (d) $A = 1$. The green (top) and red (bottom) areas designate regions where solely the FHS or FHA mode is stable, respectively. The bistability (coexistence of these stable modes) occurs in the yellow (middle) region. In the blank area, no stable modes of these types are found (in fact, an unstable FHS mode exists in this area). In panels (a) and (b), the dashed lines represent the analytical prediction (15), $P = 2\pi|1/2 - \omega|$, for the existence boundary of the FHA mode (the prediction is relevant at small values of $|1/2 - \omega|$, P , and A). The horizontal dotted line in (c) is the cross section of the bistability region, along which energies of the FHS and FHA modes is compared in Fig. III B(a).

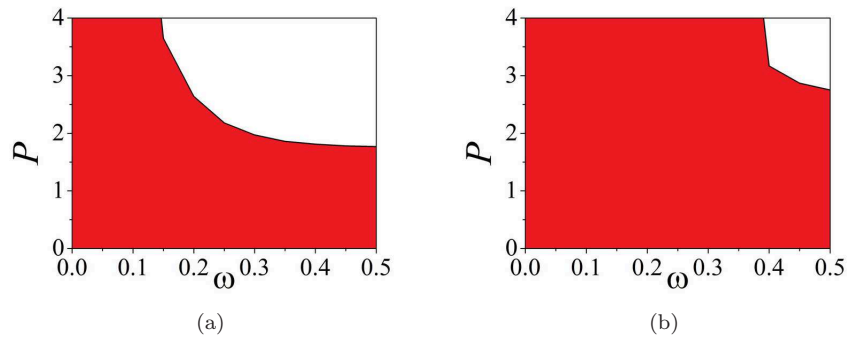


FIG. 7: (Color online) In the case of the SF nonlinearity, the AnS (antisymmetric) mode exists and is stable in the red area, as shown here for (a) $A = 0.2$ and $A = 0.4$ (b).

comparison along the horizontal dotted line, which is drawn in Fig. 6(c), is presented in Fig. 8(a). The figure clearly shows the following relation between the energies:

$$H_{\text{FHA}} < H_{\text{AnS}} < H_{\text{FHS}}. \quad (18)$$

For the 2HS and 2HA patterns, which are based on the second angular harmonic, Fig. 9 displays the stability areas in the (P, ω) plane, at different values of the lattice's strength, A [cf. Fig. 6], together with the stability area for the

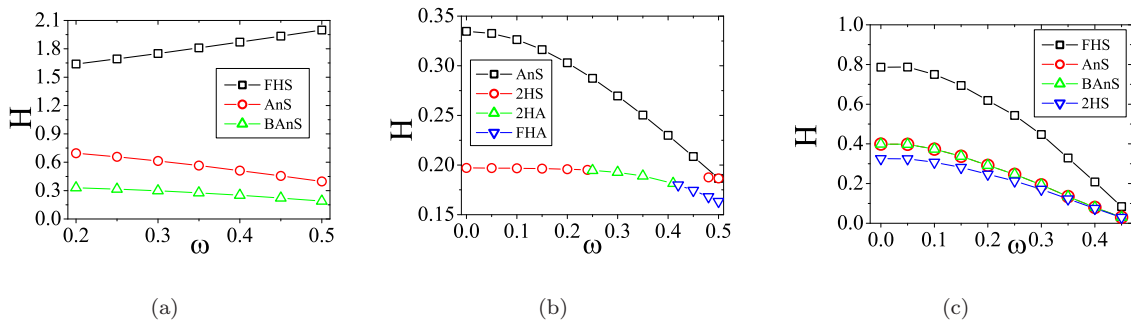


FIG. 8: (Color online) (a) Energies of the FHS, FHA, and AnS modes, computed according to Eq. (6) along the horizontal dotted line drawn in Fig. 6(c), with $(P, A) = (1.25, 0.5)$, in the interval of $0.2 \leq \omega \leq 0.5$. (b) The energies of the 2HS, 2HA, and FHA modes, along with the coexisting AnS one, along the horizontal dotted line drawn in Fig. 9(c), for $(P, A) = (0.5, 0.5)$. Panels (a) and (b) pertain to the system with the SF nonlinearity, $\sigma = +1$. (c) The energies of the AnS, BAnS (broken-antisymmetry), and 2HS modes, along the boundary separating the existence regions of the AnS and BAnS solutions in the case of the SDF nonlinearity ($\sigma = -1$), see Fig. 12(b).

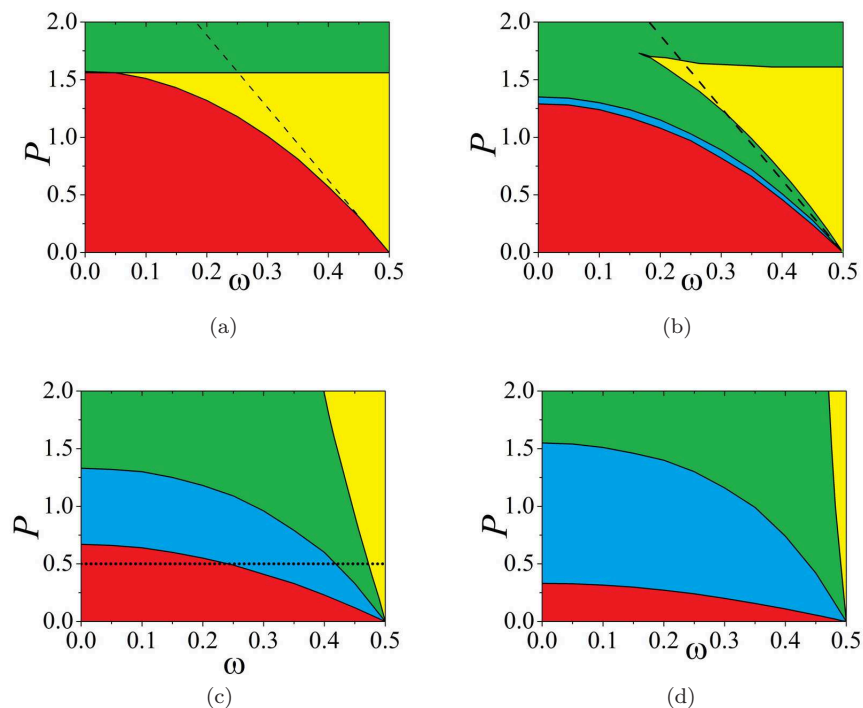


FIG. 9: (Color online) The same as in Fig. 6, but for the following types of the solutions. The green (top) area: the stable FHA mode; the red (bottom) area: the stable 2HS mode; the blue (intermediate) area: the stable 2HA mode; the yellow (rightmost) area: the bistability of the FHA and 2HS modes.

FHA mode, which may stably coexist with the 2HS pattern. Figure 9 also demonstrates that, as mentioned above, the 2HA mode, which exists and is stable in the blue (intermediate) area in Fig. 9, does not exist at $A = 0$, emerging and expanding with the increase of A . Note that, on the contrary to the situation for the patterns dominated by the fundamental angular harmonic (FHS and FHA) described above, there is no overlap between the stability areas of the symmetric and asymmetric second-harmonic-based modes, 2HS and 2HA, hence (as confirmed by an additional consideration of the numerical results) the symmetry-breaking $2HS \rightarrow 2HA$ transition, following the increase of P at $A \neq 0$, amounts to a *supercritical* bifurcation, which features no bistability [15], [2].

Another peculiarity of the symmetric mode based on the second harmonic (2HS) is that it is stable in two *disjoint* stability areas—the red and yellow ones in Fig. 9 (the bottom and rightmost regions), in the latter one the 2HS

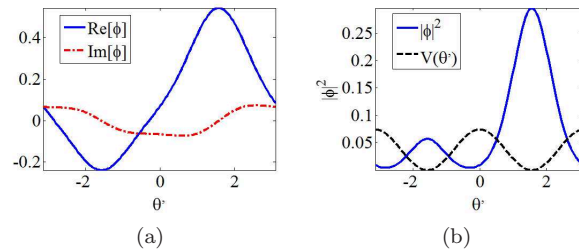


FIG. 10: (Color online) A typical example of a stable BAnS mode (the one with the *broken antisymmetry*) in the system with the SDF (self-defocusing) nonlinearity, $\sigma = -1$, and parameters $(\omega, A, P) = (0.2, 1, 0.5)$: (a) the real and imaginary parts of the stationary solution; (b) its intensity profile, which features unequal peaks in the two potential wells.

featuring the bistability with the FHA mode, although they are not linked by any bifurcation. On the other hand, there is no overlap between the stability areas of the asymmetric modes based on the different angular harmonics, FHA and 2HA, therefore these modes may be generated by the same input waveform $(1 + \sin \theta')$, in Table 1), in different parameter regions.

The effective bistability occurring in Fig. 9 makes it necessary to compare the energy of the coexisting stable patterns, which is done in Fig. 8(b), along the horizontal dotted line drawn in Fig. 9(c). The energy of the coexisting stable AnS mode is included too. In particular, the short segment corresponding to the 2HS mode appears, above the one pertaining to the FHA mode, when the horizontal dotted line in Fig. 9(c) enters the yellow (rightmost) region of the 2HS-FHA bistability. Thus, adding the results from Fig. 8(b), we extend energy relations (18) as follows:

$$H_{\text{FHA}} \text{ or } H_{2\text{HA}} < H_{2\text{HS}} < H_{\text{AnS}} < H_{\text{FHS}}. \quad (19)$$

The conclusion is that the asymmetric modes, either FHA or 2HA, represent the *ground state* of the rotating ring carrying the harmonic potential and SF nonlinearity.

IV. NUMERICAL RESULTS FOR THE SELF-DEFOCUSING NONLINEARITY ($\sigma = -1$)

In the case of the SDF nonlinearity, symmetric modes of the FHS and 2HS types have been found too, although, on the contrary to the system with the SF sign, they do not undergo any bifurcations, hence the FHA and 2HA species do not exist in this case. On the other hand, the AnS mode features an *antisymmetry-breaking* bifurcation, which gives rise to a *broken-antisymmetry* (BAnS) mode (which does not exist under the SF nonlinearity). A typical example of the stable BAnS mode is displayed in Fig. 10. In fact, antisymmetry-breaking bifurcations are characteristic to the double-well systems with the SDF nonlinearity [8]. The stationary solutions of the BAnS type can be numerically generated by the initial guess of the form of $(b + \sin \theta')$, with $0 < b \leq 1$, see Table 1.

Proceeding to the systematic description of the modes supported by the SDF nonlinearity acting in the combination with the rotating harmonic potential, we note, first, that the numerical analysis demonstrates the existence and stability of the mode of the 2HS type at all values of (ω, P, A) , therefore this solution is not included in the stability diagrams, which are displayed for the FHS mode in Fig. 12, and for the AnS and newly found BAnS ones in Fig. 11.

In the blank area of Fig. 12, the FHS solutions exist too, featuring an instability accounted for by a quartet of complex eigenvalues [see Eq. (17)]. In direct simulations, this instability converts the stationary mode into an oscillatory one (not shown here). Further, Fig. 12 shows that the antisymmetry-breaking transition, which follows the increase of the total power, P , is of a supercritical type. Actually, the supercritical character of the antisymmetry-breaking bifurcation is a characteristic feature of systems with the SDF sign of the nonlinearity [8].

Finally, the energy comparison for the model with the SDF nonlinearity is presented in Fig. 8(c), along the boundary separating the existence (and stability) regions of the AnS and BAnS modes in Fig. 12(b). The figure shows the energies of these modes, which coincide along the boundary, along with the results for the FHS and 2HS symmetric modes. From here, it is concluded that the energies are related as follows:

$$H_{2\text{HS}} < H_{\text{BAnS}} = H_{\text{AnS}} < H_{\text{FHS}}, \quad (20)$$

i.e., the 2HS mode represents the *ground state* in the case of the SDF nonlinearity, cf. Eqs. (18) and (19).

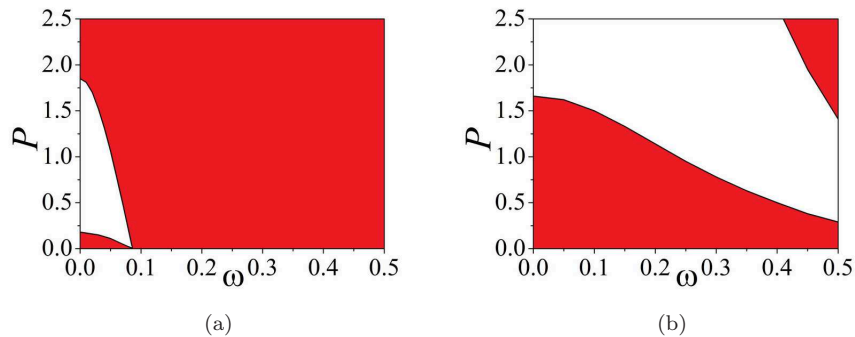


FIG. 11: (Color online) The stability diagram for the FHS mode, in the case of the SDF nonlinearity ($\sigma = -1$), in the (ω, P) plane, for $A = 1.2$ (a) and $A = 1.75$ (b). The FHS modes are stable and unstable in the red and blank areas, respectively.

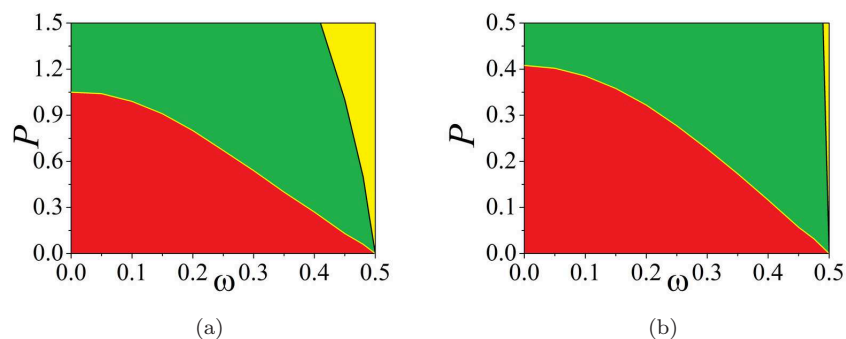


FIG. 12: (Color online) The stability diagrams for the AnS (antisymmetric) and BAnS (*broken-antisymmetry*) modes in the case of the SDF nonlinearity for $A = 0.5$ (a) and $A = 1$ (b). The red (bottom) and green (top) areas refer to the monostability of the AnS and BAnS modes, respectively. The bistability between these species occurs in the yellow (rightmost) region.

V. CONCLUSION

The objective of this work is to study the trapped modes of the symmetric, asymmetric, and antisymmetric types, and the symmetry- or antisymmetry-breaking transitions between them, in the rotating ring carrying the DWP (double-well potential) and the cubic nonlinearity with the SF or SDF (self-focusing or defocusing) sign. The analysis has been performed in the first rotational Brillouin zone. In the SF case, five types of different modes, and their stability, have been identified, three dominated by the fundamental angular harmonic (FHS, FHA, and AnS), and two others based on the second harmonic, 2HS and 2HA modes. The SSB (spontaneous symmetry-breaking) transition between the FHS and FHA modes is of the subcritical type, featuring a conspicuous bistability area, while the transition between the 2HS and 2HA states is supercritical. There is no overlap between the existence regions of the asymmetric modes of the FHA and 2HA types, one of which realizes the ground state of the SF system.

The SDF model supports four distinct species of the trapped modes, *viz.*, FHS, 2HS, AnS, and, in addition, the BAnS (broken-antisymmetry) mode. The latter one appears from the AnS state as a result of supercritical antisymmetry-breaking transition. The 2HS mode represents the ground state of the SDF system.

The present work can be naturally extended in other directions. First, it is possible to consider the rotating potential in the form of $A \cos(n\theta')$ with $n \geq 3$, while the present analysis corresponds to the DWP with $n = 2$ [note that Eq. (1) suggests a possibility to create the helical photonic lattice with $n = 2S$ and $S > 1$]. This generalization will give rise to many new trapped modes; in particular, it may be possible to build one with a small width, $\Delta\theta' \ll 2\pi$, hence it may be considered as a *soliton* trapped in the lattice and rotating along with it, cf. Ref. [24]. It is relevant too to consider effects of the two-dimensionality (the entire rotating plane, rather than a narrow ring). Our preliminary analysis, based on simulations of the 2D counterpart of Eq. (3), demonstrates essentially the same types of trapped modes in rotating annuli of a finite radial size, as reported above in the one-dimensional limit. Another interesting extension is to replace the linear rotating potential by its nonlinear counterpart, generated by modulation of the local nonlinearity along the angular coordinate (as was done in Ref. [43] in the absence of the rotation). Results obtained

for one-dimensional modes trapped in the rotating nonlinear potential will be reported elsewhere.

Acknowledgments

We appreciate help in the use of numerical methods provided by Nir Dror and Shenhe Fu. This work was supported by Chinese agencies NKBRFSF (grant No. G2010CB923204) and CNNSF (grant No. 11104083, 10934011), by the German-Israel Foundation through grant No. I-1024-2.7/2009, and by the Tel Aviv University in the framework of the “matching” scheme.

-
- [1] J. C. Eilbeck, P. S. Lomdahl, and A. C. Scott, *Physica D* **16**, 318 (1985).
- [2] A. W. Snyder, D. J. Mitchell, L. Poladian, D. R. Rowland, and Y. Chen, *J. Opt. Soc. Am. B* **8**, 2102 (1991); C. Paré and M. Fłrjańczyk, *Phys. Rev. A* **41**, 6287 (1990); A. I. Maimistov, *Kvantovaya Elektron.* **18**, 758 (1991); *Sov. J. Quantum Electron.* **21**, 687 (1991); N. Akhmediev and A. Ankiewicz, *Phys. Rev. Lett.* **70**, 2395 (1993); P. L. Chu, B. A. Malomed, and G. D. Peng, *J. Opt. Soc. Am. B* **10**, 1379 (1993); B. A. Malomed, in *Progress Optics*, edited by E. Wolf, Vol. 43 (North Holland, Amsterdam, 2002), p. 71.
- [3] W. C. K. Mak, B. A. Malomed, and P. L. Chu, *J. Opt. Soc. Am. B* **15**, 1685 (1998).
- [4] J. W. Fleischer, M. Segev, N. K. Efremidis, and D. N. Christodoulides, *Nature* **422**, 147 (2003); X. Wang and Z. Chen, *Phys. Rev. Lett.* **96**, 083904(2006); S. Jia and J. W. Fleischer, *Phys. Rev. A* **79**, 041804(R) (2009).
- [5] P. G. Kevrekidis, Z. Chen, B. A. Malomed, D. J. Frantzeskakis, and M. I. Weinstein, *Phys. Lett. A* **340**, 275 (2005).
- [6] G. J. Milburn, J. Corney, E. M. Wright, and D. F. Walls, *Phys. Rev. A* **55**, 4318 (1997); K. W. Mahmud, H. Perry, and W. P. Reinhardt, *Phys. Rev. A* **71**, 023615 (2005); T. Schumm, S. Hofferberth, L. M. Andersson, S. Wildermuth, S. Groth, I. Bar-Joseph, J. Schmiedmayer and P. Krüger, *Nature Physics* **1**, 57 (2005); D. R. Dounas-Frazer, A. M. Hermundstad, and L. D. Carr, *Phys. Rev. Lett.* **99**, 200402 (2007); Y. P. Huang and M. G. Moore, *Phys. Rev. Lett.* **100**, 250406 (2008); Q. Y. He, M. D. Reid, T. G. Vaughan, C. Gross, M. Oberthaler, and P. D. Drummond, *Phys. Rev. Lett.* **106**, 120405 (2011).
- [7] I. Zapata, F. Sols, and A. J. Leggett, *Phys. Rev. A* **57**, R28 (1998), L. Radzihovsky and V. Gurarie, *Phys. Rev. A* **81**, 063609 (2010); R. Qi, X. L. Yu, Z. B. Li, and W. M. Liu, *Phys. Rev. Lett.* **102**, 185301 (2009).
- [8] M. Matuszewski, B. A. Malomed, and M. Trippenbach, *Phys. Rev. A* **75**, 063621 (2007); M. Trippenbach, E. Infeld, J. Gocalek, M. Matuszewski, M. Oberthaler, and B. A. Malomed, *Phys. Rev. A* **78**, 013603 (2008).
- [9] G. Mazzarella, B. Malomed, L. Salasnich, M. Salerno, and F. Toigo, *J. Phys. B: At. Mol. Opt. Phys.* **44**, 035301 (2011).
- [10] H. T. Ng and P. T. Leung, *Phys. Rev. A* **71**, 013601 (2005); I. I. Satija, R. Balakrishnan, P. Naudus, J. Heward, M. Edwards, and C. W. Clark, *Phys. Rev. A* **79**, 033616 (2009); C. Wang, P. G. Kevrekidis, N. Whitaker, and B. A. Malomed, *Physica D* **237**, 2922(2008).
- [11] M. Albiez, R. Gati, J. Fölling, S. Hunsmann, M. Cristiani, and M. K. Oberthaler, *Phys. Rev. Lett.* **95**, 010402 (2005); R. Gati, M. Albiez, J. Fölling, B. Hemmerling, and M. K. Oberthaler, *Appl. Phys. B* **82**, 207 (2006).
- [12] A. Gubeskys and B. A. Malomed, *Phys. Rev. A* **75**, 063602 (2007); *ibid.* **76**, 043623 (2007); L. Salasnich, B. A. Malomed, and F. Toigo, *ibid.* **81**, 045603 (2010).
- [13] S. K. Adhikari, B. A. Malomed, L. Salasnich, and F. Toigo, *Phys. Rev. A* **81**, 053630 (2010).
- [14] E. A. Ostrovskaya, Y. S. Kivshar, M. Lisak, B. Hall, F. Cattani, and D. Anderson, *Phys. Rev. A* **61**, 031601(2000); R. D’Agosta, B. A. Malomed, C. Presilla, *Phys. Lett. A* **275**, 424 (2000); R. K. Jackson and M. I. Weinstein, *J. Stat. Phys.* **116**, 881 (2004); D. Ananikian and T. Bergeman, *Phys. Rev. A* **73**, 013604 (2006); E. W. Kirr, P. G. Kevrekidis, E. Shlizerman, and M. I. Weinstein, *SIAM J. Math. Anal.* **40**, 566 (2008).
- [15] G. Iooss and D. D. Joseph, *Elementary Stability and Bifurcation Theory* (Springer: New York, 1980).
- [16] Y. S. Kivshar and G. P. Agrawal, *Optical Solitons: From Fibers to Photonic Crystals* (Academic Press: San Diego).
- [17] A. E. Fetter, *Rev. Mod. Phys.* **81**, 647 (2009).
- [18] P. Engels, I. Coddington, P. C. Haljan, V. Schweikhard, and E. A. Cornell, *Phys. Rev. Lett.* **90**, 170405 (2003).
- [19] A. L. Fetter, *Phys. Rev. A* **64**, 063608 (2001); E. Lundh, *ibid.* **65**, 043604 (2002); K. Kasamatsu, M. Tsubota, and M. Ueda, *ibid.* **66**, 053606 (2002); G. M. Kavoulakis and G. Baym, *New J. Phys.* **5**, 51 (2003); A. Aftalion and I. Danaila, *Phys. Rev. A* **69**, 033608 (2004); U. R. Fischer and G. Baym, *Phys. Rev. Lett.* **90**, 140402 (2003); A. D. Jackson and G. M. Kavoulakis, *Phys. Rev. A* **70**, 023601 (2004); T. K. Ghosh, *ibid.* **69**, 043606 (2004).
- [20] N. K. Wilkin, J. M. F. Gunn, and R. A. Smith, *Phys. Rev. Lett.* **80**, 2265 (1998); B. Mottelson, *ibid.* **83**, 2695 (1999); C. J. Pethick and L. P. Pitaevskii, *Phys. Rev. A* **62**, 033609 (2000); E. Lundh, A. Collin, and K.-A. Suominen, *Phys. Rev. Lett.* **92**, 070401 (2004); G. M. Kavoulakis, A. D. Jackson, and G. Baym, *Phys. Rev. A* **70**, 043603 (2004); A. Collin, *ibid.* **73**, 013611 (2006); A. Collin, E. Lundh, and K.-A. Suominen, *Phys. Rev. A* **71**, 023613 (2005); S. Bargi, G. M. Kavoulakis, and S. M. Reimann, *ibid.* **73**, 033613 (2006); H. Sakaguchi and B. A. Malomed, *ibid.* **78**, 063606 (2008).
- [21] V. Schweikhard, I. Coddington, P. Engels, S. Tung, and E. A. Cornell, *Phys. Rev. Lett.* **93**, 210403 (2004); S. Tung, V. Schweikhard, and E. A. Cornell, *ibid.* **97**, 240402 (2006).
- [22] G. Kakarantzas, A. Ortigosa-Blanch, T. A. Birks, P. St. J. Russell, L. Farr, F. Couny, and B. J. Mangan, *Opt. Lett.* **28**, 158

- (2003).
- [23] J. W. Reijnders and R. A. Duine, Phys. Rev. A **71**, 063607 (2005); H. Pu, L. O. Baksmaty, S. Yi, and N. P. Bigelow, Phys. Rev. Lett. **94**, 190401 (2005); R. Bhat, L. D. Carr, and M. J. Holland, *ibid.* **96**, 060405 (2006); K. Kasamatsu and M. Tsubota, *ibid.* **97**, 240404 (2006).
- [24] H. Sakaguchi and B. A. Malomed, Phys. Rev. A **75**, 013609 (2007); H. Sakaguchi and B. A. Malomed, Phys. Rev. A **79**, 043606 (2009).
- [25] Y. V. Kartashov, B. A. Malomed, and L. Torner, Phys. Rev. A **75**, 061602(R) (2007).
- [26] V. A. Brazhnyi and V. V. Konotop, Mod. Phys. Lett. B **18**, 627 (2004).
- [27] H. Saito and M. Ueda, Phys. Rev. Lett. **93**, 220402 (2004).
- [28] S. Schwartz, M. Cozzini, C. Menotti, I Carusotto, P. Bouyer, and S. Stringari, New J. Phys. **8**, 162 (2006).
- [29] R. Carretero-González, D. J. Frantzeskakis, and P. G. Kevrekidis, Nonlinearity **21**, R139 (2008).
- [30] L. H. Wen and X. B. Luo, arXiv:1204.4522 (Laser Phys. Lett., in press). L. Wen, H. Xiong, and B. Wu, Phys. Rev. A **82**, 053627 (2010).
- [31] N. K. Efremidis, S. Sears, D. N. Christodoulides, J. W. Fleischer, and M. Segev, Phys. Rev. E **66**, 046602 (2002); J. W. Fleischer, T. Carmon, M. Segev, N. K. Efremidis, and D. N. Christodoulides, Phys. Rev. Lett. **90**, 023902 (2003); J. W. Fleischer, M. Segev, N. K. Efremidis, and D. N. Christodoulides, Nature **422**, 147 (2003); H. Martin, E. D. Eugenieva, Z. G. Chen, and D. N. Christodoulides, Phys. Rev. Lett. **92**, 123902 (2004); D. N. Neshev, T. J. Alexander, E. A. Ostrovskaya, Y. S. Kivshar, H. Martin, I. Makasyuk, and Z. G. Chen, *ibid.* **92**, 123903 (2004); J. W. Fleischer, G. Bartal, O. Cohen, O. Manela, M. Segev, J. Hudock, and D. N. Christodoulides, *ibid.* **92**, 123904 (2004); B. Freedman, G. Bartal, M. Segev, R. Lifshitz, D. N. Christodoulides, and J. W. Fleischer, Nature **440**, 1166 (2006); H. Trompeter, W. Królikowski, D. N. Neshev, A. S. Desyatnikov, A. A. Sukhorukov, Y. S. Kivshar, T. Pertsch, U. Peschel, and F. Lederer, Phys. Rev. Lett. **96**, 053903 (2006); R. Fischer, D. Trager, D. N. Neshev, A. A. Sukhorukov, W. Królikowski, C. Denz, and Y. S. Kivshar, *ibid.* **96**, 023905 (2006); T. Schwartz, G. Bartal, S. Fishman, and M. Segev, Nature **446**, 52 (2007).
- [32] J. W. Fleischer, G. Bartal, O. Cohen, T. Schwartz, O. Manela, B. Freedman, M. Segev, H. Buljan, N. K. Efremidis, Opt. Exp. **13**, 1780 (2005); F. Lederer, G. I. Stegeman, D. N. Christodoulides, G. Assanto, M. Segev, and Y. Silberberg, Phys. Rep. **463**, 1 (2008).
- [33] M. Fleischhauer, A. Imamoğlu, and J. P. Marangos, Rev. Mod. Phys. **77**, 633 (2005); H. Schmidt and A. Imamoğlu, Opt. Lett. **21**, 1936 (1996); H. Wang, D. Goorskey, and M. Xiao, Phys. Rev. Lett. **87**, 073601 (2001).
- [34] Y. Li, B. A. Malomed, M. Feng, and J. Zhou, Phys. Rev. A **82** 063813 (2010); W. Pang, J. Wu, Z. Yuan, Y. Liu and G. Chen, J. Phys. Soc. Jpn. **80**, 113401 (2011); J. Wu, M. Feng, W. Pang, S. Fu, and Y. Li, J. Nonlin. Opt. Phys. **20**, 193 (2011); Y. Li, W. Pang, S. Fu, and B. A. Malomed, Phys. Rev. A **85**, 053821 (2012).
- [35] E. Kuznetsova, O. Kocharovskaya, P. R. Hemmer, and M. O. Scully, Phys. Rev. A **66**, 063802 (2002); A. V. Turukhin, V. S. Sudarshanam, M. S. Shahriar, J. A. Musser, B. S. Ham, and P. R. Hemmer, Phys. Rev. Lett. **88**, 023602 (2002).
- [36] S. Gupta, K. W. Murch, K. L. Moore, T. P. Purdy, and D. M. Stamper-Kurn, Phys. Rev. Lett. **95**, 143201 (2005); A. S. Arnold, C. S. Garvie, and E. Riis, Phys. Rev. A **73**, 041606(R) (2006); I. Lesanovsky and W. von Klitzing, *ibid.* **99**, 083001 (2007); C. Ryu, M. F. Andersen, P. Cladé, V. Natarajan, K. Helmerson, and W. D. Phillips, Phys. Rev. Lett. **99**, 260401 (2007); A. Ramanathan, K. C. Wright, S. R. Muniz, M. Zelan, W. T. Hill III, C. J. Lobb, K. Helmerson, W. D. Phillips, and G. K. Campbell, *ibid.* **106**, 130401 (2011).
- [37] L. Salasnich, A. Parola, and L. Reatto, Phys. Rev. A **74**, 031603(R) (2006); R. Kanamoto, H. Saito, and M. Ueda, *ibid.* **73**, 033611 (2006); M. Modugno, C. Tozzo, and F. Dalfovo, *ibid.* **74**, 061601 (R) (2006); R. Bhat, M. J. Holland, and L. D. Carr, Phys. Rev. Lett. **96**, 060405 (2006); A. V. Carpentier and H. Michinel, EPL **78**, 10002 (2007); P. Mason and N. G. Berloff, Phys. Rev. A **79**, 043620 (2009); J. Brand, T. J. Haigh, and U. Zülicke, *ibid.* **80**, 011602 (R) (2009); P. Capuzzi and D. M. Jezek, J. Phys. B: At. Mol. Opt. Phys. **42**, 145301 (2009); A. Aftalion and P. Maso, *ibid.* **81**, 023607 (2010); J. Smyrnakis, M. Magiropoulos, G. M. Kavoulakis, and A. D. Jackson, *ibid.* **81**, 063601 (2010); S. Zöllner, G. M. Bruun, C. J. Pethick, and S. M. Reimann, Phys. Rev. Lett. **107**, 035301 (2011); Z.-W. Zhou, S.-L. Zhang, X.-F. Zhou, G.-C. Guo, X. Zhou, and H. Pu, Phys. Rev. A **83**, 043626 (2011); M. Abad, M. Guilleumas, R. Mayol, M. Pi, and D. M. Jezek, *ibid.* **84**, 035601 (2011); X. Zhou, S. Zhang, Z. Zhou, B. A. Malomed, and H. Pu, *ibid.* **85**, 023603 (2012); S. K. Adhikari, *ibid.* **85**, 053631 (2012).
- [38] J. Smyrnakis, S. Bargi, G. M. Kavoulakis, M. Magiropoulos, K. Kärkkäinen, and S. M. Reimann, Phys. Rev. Lett. **103**, 100404 (2009).
- [39] C. Kittel, *Introduction to Solid State Physics* (Wiley: New York,1995).
- [40] M. Vakhitov and A. Kolokolov, Izvestiya VUZov Radiofizika **16**, 1020 (1973) [in Russian; English translation: Radiophys. Quantum. Electron. **16**, 783 (1973)]; L. Bergé, Phys. Rep. **303**, 259 (1998); E. A. Kuznetsov and F. Dias, *ibid.* **507**, 43 (2011).
- [41] H. Sakaguchi and B. A. Malomed, Phys. Rev. A **81**, 013624 (2010).
- [42] J. Yang and T. I. Lakoba, Stud. Appl. Math. **118**, 153 (2007); **120**, 265 (2008).
- [43] L. C. Qian, M. L. Wall, S. Zhang, Z. Zhou, and H. Pu, Phys. Rev. A **77**, 013611 (2008); Z.-W. Zhou, S.-L. Zhang, X.-F. Zhou, G.-C. Guo, X. Zhou, and H. Pu, *ibid.* **83**, 043626 (2011); X.-F. Zhou, S.-L. Zhang, Z.-W. Zhou, B. A. Malomed, and H. Pu, *ibid.* **85**, 023603 (2012).